Spin-orbital entangled excitonic insulator with quadrupole order

Toshihiro Sato,[1,2] Tomonori Shirakawa,[3,2,4,5] and Seiji Yunoki[2,4,5]

[1]*Institut für Theoretische Physik und Astrophysik, Universität Würzburg, 97074 Würzburg, Germany*

[2]*Computational Condensed Matter Physics Laboratory, RIKEN Cluster for Pioneering Research (CPR), Wako, Saitama 351-0198, Japan*

[3]*SISSA–International School for Advanced Studies, Via Bonomea 265, 34136 Trieste, Italy*

[4]*Computational Quantum Matter Research Team, RIKEN Center for Emergent Matter Science (CEMS), Saitama 351-0198, Japan*

[5]*Computational Materials Science Research Team, RIKEN Center for Computational Science (R-CCS), Kobe, Hyogo 650-0047, Japan*

(Received 21 August 2018; revised manuscript received 7 January 2019; published 7 February 2019)

We employ the multiorbital dynamical mean-field theory to examine the ground state of a three-orbital Hubbard model with a relativistic spin-orbit coupling (SOC) at four electrons per site. We demonstrate that the interplay between the strong electron correlations and the SOC induces a Van Vleck-type nonmagnetic insulator and its magnetic exciton condensation. In the moderate electron correlation regime, the SOC induces another type of a nonmagnetic excitonic insulator, in addition to a relativistic band insulator. Most interestingly, we find that this nonmagnetic excitonic insulator exhibits a high-order multipole ordering. The characteristic features among these insulators are manifested in the momentum-resolved single-particle excitations, thus accessible by angle-resolved photoemission spectroscopy experiments.

DOI: 10.1103/PhysRevB.99.075117

I. INTRODUCTION

$5d$ transition-metal oxides have been extensively studied from theoretical and experimental aspects because the interplay between the electron correlations and the relativistic spin-orbit coupling (SOC) can induce a variety of exotic quantum states [1]. Most of the research has focused on $(t_{2g})^5$ electron systems with a single hole in the t_{2g} manifold, i.e., layered-perovskite A_2IrO_4 (A = Sr and Ba) [2–26]. Recently, the focus has started to move onto other electron fillings. Among many interesting observations, recent experiments on $(t_{2g})^4$ electron systems with two holes in the t_{2g} manifold have reported that perovskite $AOsO_3$ (A = Ca and Ba) [27,28] and post-perovskite $NaIrO_3$ [29] exhibit a nonmagnetic insulating behavior despite the first-principles calculations based on density functional theory that predict otherwise [27,29–32]. An intriguing paramagnetic insulating behavior has also been observed in double perovskite Ba_2YIrO_6 with a $(t_{2g})^4$ electronic configuration [33,34].

It is instructive to consider two limiting cases for the $(t_{2g})^4$ electron system with the SOC. When the SOC is significantly large, i.e., in the jj coupling limit of the local effective total angular momentum j, the $j = 1/2$ and $3/2$ based bands are well separated to simply become a relativistic band insulator with the fully occupied $j = 3/2$ and the completely empty $j = 1/2$ based bands. On the other hand, when the electron correlations are dominant, the LS coupling scheme in the atomic limit is a better description. According to the Hund's rule, the ground state has the orbital angular momentum $L = 1$ and the spin angular momentum $S = 1$, which couple via the SOC to form the total angular momentum $J = 0$. Considering the hybridization between neighbors, it is expected that the local singlets with $J = 0$ form a band to become a Van Vleck-type nonmagnetic insulator. In this context, Khaliullin has proposed a Van Vleck-type excitonic insulator, where an excitonic condensation between the local $J = 0$ and $J = 1$ states is driven by the magnetic order through the intersite exchange interaction [35].

The theoretical studies in the two extreme limits are important to investigate possible exotic states. In addition, it is highly desirable to examine the electronic ground state as well as the excitations in a wider range of couplings using a numerical technique that allows us to treat the interplay between the electron correlations and the SOC in a well-controlled manner.

For this purpose, here we employ the multiorbital dynamical mean-field theory (DMFT) [36] to study a three-orbital Hubbard model with the SOC at four electrons per site, corresponding to the $(t_{2g})^4$ electronic configuration. We determine the phase diagram of the intraorbital Coulomb interaction U versus the SOC λ plane in the model, which is summarized in Fig. 1. We find that the phase diagram displays four phases, i.e., metal, nonmagnetic excitonic insulator, antiferromagnetic excitonic insulator, and nonmagnetic insulator. Moreover, the interplay between U and λ can realize two types of the nonmagnetic insulator: a Van Vleck-type nonmagnetic insulator and a relativistic band insulator. Most interestingly, we find that the nonmagnetic excitonic insulator exhibits quadrupole order.

The rest of this paper is organized as follows. After briefly introducing the model and numerical method in Sec. II, the ground-state phase diagram is first determined in Sec. III. The possibility of multipole orderings in the nonmagnetic phases are separately examined in Sec. IV. The single-particle excitations for four different insulating states are also studied in Sec. V. The paper is concluded with summary in Sec. VI.

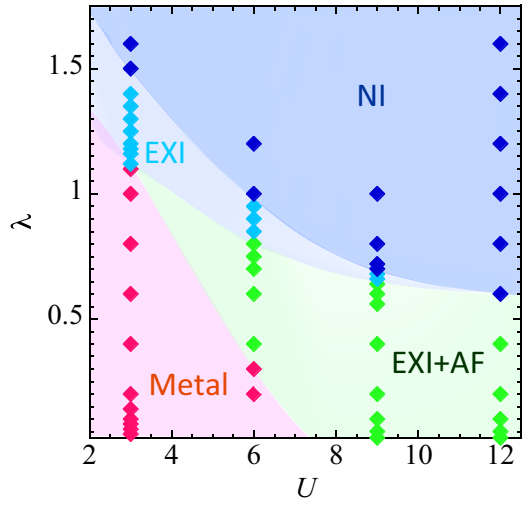

FIG. 1. Schematic U-λ phase diagram at $T = 0.06$. EXI, EXI+AF, and NI stand for nonmagnetic excitonic insulating phase, antiferromagnetic excitonic insulating phase, and nonmagnetic insulating phase, respectively. In the NI, a Van Vleck-type nonmagnetic insulator is smoothly connected to a relativistic band insulator that appears in the limit of large SOC. The EXI+AF shows nonzero diploe moment, i.e., magnetically ordered, while the EXI displays quadrupole order with zero diploe moment. Diamonds with different colors, corresponding to four different phases, indicate the parameter sets for which the calculations are performed to determine the nature of states.

II. MODEL AND METHOD

A. Model

The three-orbital Hubbard model with the relativistic SOC studied here is given as

$$H = H_0 + H_{\rm I}, \tag{1}$$

where the noninteracting part is represented by

$$H_0 = \sum_{\langle i,i'\rangle}\sum_{\gamma,\sigma} t^{\gamma} c^{\dagger}_{i\gamma\sigma} c_{i'\gamma\sigma} - \mu \sum_{i,\gamma,\sigma} n^{\gamma}_{i\sigma} + H_{\rm SO} \tag{2}$$

and the local two-body interacting part is described by

$$\begin{aligned} H_{\rm I} = {} & U \sum_{i,\gamma} n^{\gamma}_{i\uparrow} n^{\gamma}_{i\downarrow} + \frac{U' - J_{\rm H}}{2} \sum_{i,\gamma\neq\delta,\sigma} n^{\gamma}_{i\sigma} n^{\delta}_{i\sigma} \\ & + \frac{U'}{2} \sum_{i,\gamma\neq\delta,\sigma} n^{\gamma}_{i\sigma} n^{\delta}_{i\bar{\sigma}} - J_{\rm H} \sum_{i,\gamma\neq\delta} c^{\dagger}_{i\gamma\uparrow} c_{i\gamma\downarrow} c^{\dagger}_{i\delta\downarrow} c_{i\delta\uparrow} \\ & + J_{\rm P} \sum_{i,\gamma\neq\delta} c^{\dagger}_{i\gamma\uparrow} c^{\dagger}_{i\gamma\downarrow} c_{i\delta\downarrow} c_{i\delta\uparrow}. \end{aligned} \tag{3}$$

In the noninteracting part H_0, t^{γ} sets the nearest-neighbor hopping amplitude for t_{2g} orbitals $\gamma = (d_{yz}, d_{zx}, d_{xy})$, $c^{\dagger}_{i\gamma\sigma}$ is an electron creation operator at site i with orbital γ and spin σ ($=\uparrow,\downarrow$), and $n^{\gamma}_{i\sigma} = c^{\dagger}_{i\gamma\sigma} c_{i\gamma\sigma}$. Notice that the electron hopping considered here is diagonal for the three orbitals with the same amplitude, as defined below, and thus the hopping term preserves the spherical symmetry. The chemical potential μ is tuned to be at four electrons per site. The SOC term $H_{\rm SO}$ is given as

$$\begin{aligned} H_{\rm SO} &= \lambda \sum_{i} \sum_{\gamma,\delta} \sum_{\sigma,\sigma'} \langle\gamma|\mathbf{l}|\delta\rangle \cdot \langle\sigma|\mathbf{s}|\sigma'\rangle c^{\dagger}_{i\gamma\sigma} c_{i\delta\sigma'} \\ &= \frac{\lambda}{2} \sum_{i,\sigma} \left(c^{\dagger}_{id_{yz}\sigma}, c^{\dagger}_{id_{zx}\sigma}, c^{\dagger}_{id_{xy}\bar{\sigma}} \right) \\ &\quad \times \begin{pmatrix} 0 & is_{\sigma} & -s_{\sigma} \\ -is_{\sigma} & 0 & i \\ -s_{\sigma} & -i & 0 \end{pmatrix} \begin{pmatrix} c_{id_{yz}\sigma} \\ c_{id_{zx}\sigma} \\ c_{id_{xy}\bar{\sigma}} \end{pmatrix}, \end{aligned} \tag{4}$$

where λ is the SOC, $\mathbf{l}$ ($\mathbf{s}$) is the local orbital (spin) angular momentum operator at each site, $s_{\sigma} = 1\,(-1)$ for $\sigma = \uparrow$ ($\downarrow$), and $\bar{\sigma}$ implies the opposite spin of σ. Here, we have assumed the local cubic symmetry. The interacting part $H_{\rm I}$ includes the intraorbital (interorbital) Coulomb interaction U (U'), the Hund's rule coupling $J_{\rm H}$, and the spin flip and pair hopping coupling $J_{\rm P}$. Because of the spherical symmetry in the atomic limit, we impose $U' = U - 2J_{\rm H}$ and $J_{\rm H} = J_{\rm P}$ [37,38]. In this paper, we set $J_{\rm H} = 0.15U$, which is within the range for typical transition-metal compounds [39,40].

B. Method

The main focus in this study is to explore the possible ordered states appearing as a results of competition between the electron correlations and the SOC. To take into account strong electron correlations and magnetic fluctuations in the three orbitals, here we use the cluster DMFT employing a three-orbital cluster (multiorbital DMFT). In this study, the electron correlations and magnetic fluctuations as well as possible ordered states are treated by the multiorbital DMFT on the Bethe lattice with coordination number $Z \to \infty$ [41,42], for which the DMFT is exact. Moreover, we consider the same bandwidth W for the three orbitals (i.e., $t^{\gamma} = t/\sqrt{Z}$) and set $W = 4t$. In the following, t is used as the energy unit and we show the results for the lowest temperature $T = 0.06$, which essentially represent the ground state.

In the multiorbital DMFT calculation, we numerically obtain the imaginary-time (τ) Green's functions at the impurity site, $G^{\delta,\sigma'}_{\gamma,\sigma}(i,\tau) \equiv -\langle T_{\tau} c_{i\gamma\sigma}(\tau) c^{\dagger}_{i\delta\sigma'}(0)\rangle$, by using a continuous-time quantum Monte Carlo (CTQMC) method based on the strong coupling expansion [43]. Although the CTQMC calculation in principle enables us to solve the model exactly, the negative sign problem is one of the serious issues, particularly at low temperatures for large SOC. Our previous study for the three-orbital Hubbard model with $(t_{2g})^5$ electrons [25] has demonstrated that the sign problem is improved significantly by transforming the t_{2g} orbital bases ($c_{i\gamma\sigma}$) to the maximally spin-orbit-entangled j bases (a_{ijm}) of the eigenstates of H_0 in the atomic limit, i.e.,

$$\begin{pmatrix} a_{i\frac{1}{2}\frac{s_{\sigma}}{2}} \\ a_{i\frac{3}{2}\frac{s_{\sigma}}{2}} \\ a_{i\frac{3}{2}\frac{-3s_{\sigma}}{2}} \end{pmatrix} = \frac{1}{\sqrt{6}} \begin{pmatrix} \sqrt{2} & -i\sqrt{2}s_{\sigma} & \sqrt{2}s_{\sigma} \\ s_{\sigma} & -i & -2 \\ -\sqrt{3}s_{\sigma} & -i\sqrt{3} & 0 \end{pmatrix} \begin{pmatrix} c_{id_{yz}\bar{\sigma}} \\ c_{id_{zx}\bar{\sigma}} \\ c_{id_{xy}\sigma} \end{pmatrix}. \tag{5}$$

We find that the same transformation can also improve the sign problem for the present $(t_{2g})^4$ electron systems. In the following, we omit the site index in the Green's function, i.e., $G^{\delta,\sigma'}_{\gamma,\sigma}(\tau) = G^{\delta,\sigma'}_{\gamma,\sigma}(i,\tau)$.

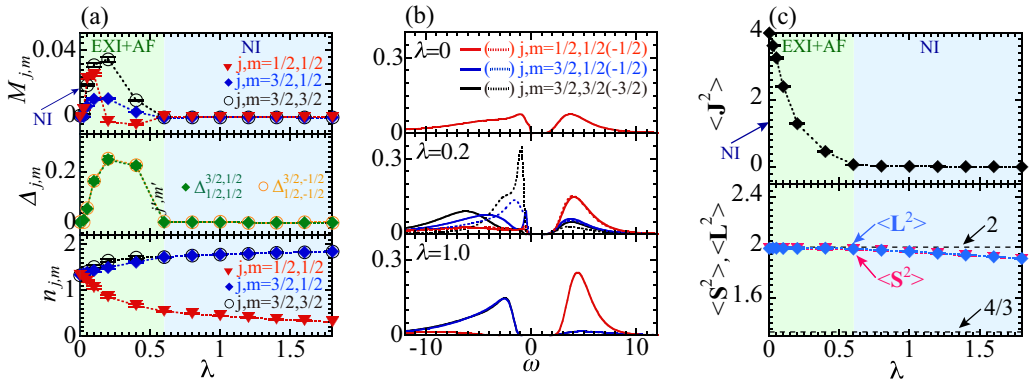

FIG. 2. (a) λ dependence of staggered magnetization $M_{j,m}$, excitonic order parameter $\Delta^{j',m'}_{j,m}$, and electron density $n_{j,m}$. (b) Single-particle excitations spectrum $A_{j,m}(\omega)$ for three different values of λ indicated in the figure. Fermi energy is located at $\omega = 0$. Note that all components of the spectra are degenerate for $\lambda = 0$, and $A_{3/2,\pm 3/2}(\omega) = A_{3/2,\pm 1/2}(\omega)$ and $A_{j,m}(\omega) = A_{j,-m}(\omega)$ for $\lambda = 1$. (c) λ dependence of total angular momentum squared $\langle \mathbf{J}^2 \rangle$ and local spin (orbital) angular momentum squared $\langle \mathbf{S}^2 \rangle$ ($\langle \mathbf{L}^2 \rangle$). All the calculations here are for $U = 12$. EXI+AF and NI stand for antiferromagnetic excitonic insulator and nonmagnetic insulator, respectively.

III. PHASE DIAGRAM

Figure 1 shows the phase diagram in the Coulomb interaction U versus the SOC λ plane. To map out the phase diagram, we investigate two ordered states. The first state considered is the magnetic order along the z direction described by the order parameter

$$M_{j,m}(l) = \frac{1}{2} \sum_{m'=\pm m} \mathrm{sign}(m') \langle a^{\dagger}_{l\,jm'} a_{l\,jm'} \rangle, \tag{6}$$

where l ($= A, B$) indicates two sublattices. Note that because our model is isotropic, the magnetic orders along the other x and y directions are identical to that along the z direction. We also consider the excitonic order described by the order parameter

$$\Delta^{j',m'}_{j,m}(l) = \langle a^{\dagger}_{l\,jm} a_{l\,j'm'} \rangle, \tag{7}$$

where $j \neq j'$ and thus the electron-hole pair is formed in different j orbitals. In addition, we calculate the electron density $n_{j,m}(l) = \sum_{m'=\pm m} \langle a^{\dagger}_{l\,jm'} a_{l\,jm'} \rangle$. We have found that $M_{j,m}(A) = -M_{j,m}(B)$, $\Delta^{j',m'}_{j,m}(A) = -\Delta^{j',-m'}_{j,-m}(B)$, and $n_{j,m}(A) = n_{j,-m}(B)$. To simplify the notation, we omit the sublattice index l in these quantities below.

We should note here that the electron hopping is still diagonal for the j bases and thus the number of electrons in each j band is conserved for the noninteracting system described by H_0. Thereby, the excitonic order is a consequence of symmetry breaking of the U(1) symmetry in which the electron-hole pair of the j bands is condensed, while the antiferromagnetic order is characterized by the broken SO(3) symmetry. In the following, we show the representative results for large and moderate values of U to construct the phase diagram shown in Fig. 1.

A. Large U case

We first examine a case with large U. Figure 2(a) shows $M_{j,m}$, $\Delta^{j',m'}_{j,m}$, and $n_{j,m}$ for $U = 12$ as a function of λ. When $\lambda = 0$, there are no magnetic and excitonic orders with $n_{j,m} = 4/3$. However, as soon as λ is finite, the excitonic order parameters become finite with $\Delta^{3/2,1/2}_{1/2,1/2} = \Delta^{3/2,-1/2}_{1/2,-1/2} \neq 0$. Concomitantly, the magnetic order parameters are also finite for all three j components and are antiferromagnetically aligned. This phase extends up to $\lambda = 0.6$. It should also be noticed that $n_{3/2,1/2} \neq n_{3/2,3/2}$ in the presence of a finite excitonic order [44]. For $\lambda \geqslant 0.6$, both magnetic and excitonic orders disappear, and $n_{3/2,1/2} = n_{3/2,3/2}$ ($n_{1/2,1/2}$) increases (decreases) towards two (zero) with further increasing λ.

Figure 2(b) shows the single-particle excitation spectrum $A_{j,m}(\omega) = -\frac{1}{\pi} \mathrm{Im} G^{j,m}_{j,m}(\omega + i0^+)$ evaluated from the imaginary-time Green's function $G^{j',m'}_{j,m}(\tau) \equiv -\langle T_\tau a_{jm}(\tau) a^{\dagger}_{j'm'}(0) \rangle$ using the maximum entropy method [45]. Here, ω is real frequency, 0^+ is infinitesimally small positive real number, and the site indices are omitted. As shown in Fig. 2(b), there is a finite excitation gap at the Fermi energy for all values of λ and therefore these states are all insulating.

To understand the nature of these insulating states, let us examine the local spin and orbital angular momenta squared, $\langle \mathbf{S}^2_i \rangle$ and $\langle \mathbf{L}^2_i \rangle$, respectively, and the local total angular momentum squared $\langle \mathbf{J}^2_i \rangle$, where

$$\mathbf{S}_i = \sum_{\gamma} \sum_{\sigma,\sigma'} \langle \sigma | \mathbf{s} | \sigma' \rangle c^{\dagger}_{i\gamma\sigma} c_{i\gamma\sigma'}, \tag{8}$$

$$\mathbf{L}_i = \sum_{\gamma,\delta} \sum_{\sigma} \langle \gamma | \mathbf{l} | \delta \rangle c^{\dagger}_{i\gamma\sigma} c_{i\delta\sigma}, \tag{9}$$

and

$$\mathbf{J}_i = \mathbf{S}_i - \mathbf{L}_i. \tag{10}$$

Since these quantities do not depend on the site index i, we simply omit this index hereafter. First, it is highly instructive to consider four limiting cases. According to the Hund's rule, when the electron correlation is significantly large with no SOC, we expect that $\langle \mathbf{S}^2 \rangle = \langle \mathbf{L}^2 \rangle = 2$ and $\langle \mathbf{J}^2 \rangle = 4$ because $\langle \mathbf{L} \cdot \mathbf{S} \rangle = 0$. If the SOC is introduced in this limit, the spin and orbital angular momenta are aligned antiparallel, and thus $\langle \mathbf{S}^2 \rangle = \langle \mathbf{L}^2 \rangle = 2$ and $\langle \mathbf{J}^2 \rangle = 0$. This is exactly the case for the ideal Van Vleck-type insulator. In the limit of significantly large SOC, where the ground state is expected to be the relativistic band insulator, $\langle \mathbf{S}^2 \rangle = \langle \mathbf{L}^2 \rangle = \frac{4}{3}$ and $\langle \mathbf{J}^2 \rangle = 0$.

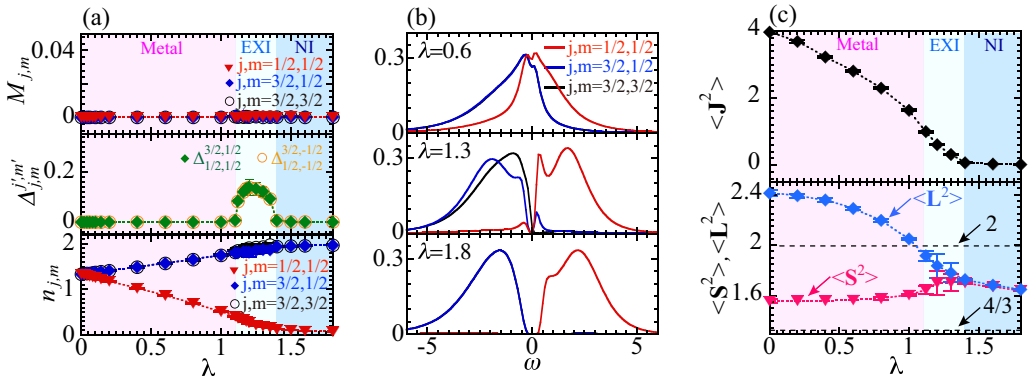

FIG. 3. (a) λ dependence of staggered magnetization $M_{j,m}$, excitonic order parameter $\Delta^{j',m'}_{j,m}$, and electron density $n_{j,m}$. (b) Single-particle excitations spectrum $A_{j,m}(\omega)$ for three different values of λ indicated in the figure. Fermi energy is located at $\omega = 0$. Note that $A_{j,m}(\omega) = A_{j,-m}(\omega)$ for $\lambda = 1.3$, and $A_{3/2,\pm 3/2}(\omega) = A_{3/2,\pm 1/2}(\omega)$ and $A_{j,m}(\omega) = A_{j,-m}(\omega)$ for other two parameters. (c) λ dependence of total angular momentum squared $\langle \mathbf{J}^2 \rangle$ and local spin (orbital) angular momentum squared $\langle \mathbf{S}^2 \rangle$ ($\langle \mathbf{L}^2 \rangle$). All the calculations here are for $U = 3$. EXI and NI stand for excitonic insulator and nonmagnetic insulator, respectively.

Finally, in the noninteracting limit without the SOC, $\langle \mathbf{S}^2 \rangle = 1.2$, $\langle \mathbf{L}^2 \rangle = 3.2$, and $\langle \mathbf{J}^2 \rangle = 4.4$.

Figure 2(c) shows the evolution of these quantities with varying λ for $U = 12$. As expected in the strong electron correlation limit, we find that $\langle \mathbf{S}^2 \rangle = \langle \mathbf{L}^2 \rangle = 2$ and $\langle \mathbf{J}^2 \rangle = 4$ for $\lambda = 0$, in accordance with the Hund's rule. With increasing λ, $\langle \mathbf{J}^2 \rangle$ monotonically decreases and eventually becomes zero for $\lambda \geqslant 0.6$, where neither magnetic nor excitonic order exists, as shown in Fig. 2(a). In this region, $\langle \mathbf{S}^2 \rangle$ and $\langle \mathbf{L}^2 \rangle$ are still close to two, specially near $\lambda = 0.6$, implying that the nonmagnetic insulator for $\lambda \geqslant 0.6$ is the Van Vleck-type insulator. However, we also notice that $\langle \mathbf{S}^2 \rangle$ and $\langle \mathbf{L}^2 \rangle$ gradually decreases with further increasing λ, while $\langle \mathbf{J}^2 \rangle$ is exactly zero, and we expect that $\langle \mathbf{S}^2 \rangle$ and $\langle \mathbf{L}^2 \rangle$ eventually become 4/3 in the limit of $\lambda \to \infty$. Namely, the Van Vleck-type insulator is smoothly connected to the simple relativistic band insulator. This nonmagnetic insulating phase is denoted as "NI" in the phase diagram shown in Fig. 1.

On the other hand, we find in the region of $0 < \lambda < 0.6$ that $\langle \mathbf{J}^2 \rangle > 0$ while $\langle \mathbf{S}^2 \rangle$ and $\langle \mathbf{L}^2 \rangle$ remain two. In this region, the magnetic and excitonic orders are both finite, and therefore we attribute this phase to the magnetic excitonic insulator (indicated as "EXI+AF" in the phase diagram shown in Fig. 1) with the enhanced hybridization between the nonmagnetic $J = 0$ state and the magnetic $J \neq 0$ excited states. Our results are in good accordance with the recent analysis based on the effective magnetic interactions in the large Coulomb interaction U [46].

B. Moderate U case

Next, we examine a case with moderate value of U, i.e., $U = 3$. It is noticed first in Fig. 3(c) that $\langle \mathbf{J}^2 \rangle$, $\langle \mathbf{S}^2 \rangle$, and $\langle \mathbf{L}^2 \rangle$ for $\lambda = 0$ clearly depart from the noninteracting values, implying that the electron correlations are indeed considered to be moderated, as it is expected for $U \approx W$. As shown in Fig. 3(a), we find no magnetic order for all values of λ. $A_{j,m}(\omega)$ exhibits quasiparticle peaks around the Fermi energy for both $j = 1/2$ and 3/2 when $\lambda < 1.2$ [see Fig. 3(b)], and thus the ground state for $\lambda < 1.2$ is metallic.

However, the quasiparticle peaks disappear with further increasing λ and the metal-insulator transition occurs at $\lambda \sim 1.2$, where the single-particle excitation gap is open. More interestingly, in the intermediate SOC region for $1.2 \leqslant \lambda \leqslant 1.4$, we find that the excitonic insulator emerges without magnetic order [see Fig. 3(a) and indicated as "EXI" in the phase diagram shown in Fig. 1]. As shown in Fig. 3(b), the degeneracy of $A_{j=3/2,m}(\omega)$ for $m = \pm 1/2$ and $\pm 3/2$ is lifted in this phase.

With further increasing λ, the excitonic order disappears for $\lambda > 1.4$ and the $j = 3/2$ based bands are almost completely occupied with a finite excitation gap to the unoccupied $j = 1/2$ based band [see Figs. 3(a) and 3(b)]. This implies that the ground state for $\lambda > 1.4$ is the relativistic band insulator. In the noninteracting limit, the SOC drives a transition from the metal to the relativistic band insulator at $\lambda = 4/3$. Therefore, the excitonic insulator found here is induced by the electron correlations just before the overlap between the $j = 1/2$ and 3/2 based bands is diminished, where the condensation of an electron-hole pair in the $j = 1/2$ and 3/2 based bands is most favorable with nonzero $\Delta^{3/2,\pm 1/2}_{1/2,\pm 1/2}$.

IV. EXCITONIC INSULATORS

We have found the two excitonic insulators, i.e., the nonmagnetic excitonic insulator for moderate U and the magnetic excitonic insulator for large U, indicated respectively as "EXI" and "EXI+AF" in the phase diagram shown in Fig. 1. The former appears between the metal and the relativistic band insulator in the phase diagram, and an electron-hole pair in the $j = 1/2$ and 3/2 based bands are condensed in this state [see Figs. 3(a) and 3(b)]. Therefore, the exciton condensation is similar to the conventional one where a valence hole and a conduction electron form a pair.

In contrast, the other excitonic insulator appears in the strong coupling regime where U alone can open the single-particle excitation gap without magnetic order (see Fig. 2 for $\lambda = 0$). As shown in Fig. 2(c), in this strong coupling regime, the LS coupling scheme is a better description and thus the excitonic insulator here, accompanying the magnetic order, is

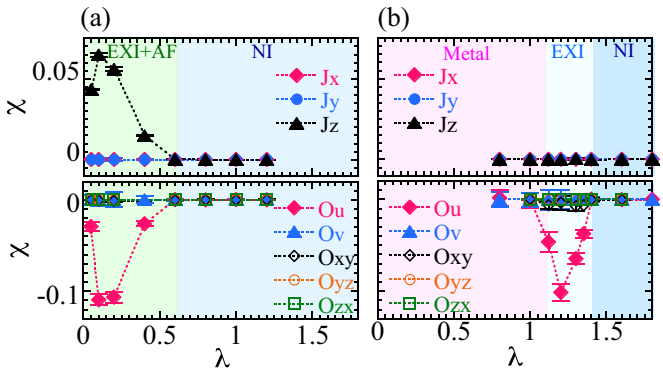

FIG. 4. λ dependence of multipole moment χ for Γ_{4u} dipoles (J_x, J_y, J_z), Γ_{3g} quadrupoles (O_u, O_v), and Γ_{5g} quadrupoles (O_{xy}, O_{yz}, O_{zx}) when (a) $U = 12$ and (b) $U = 3$. EXI, EXI+AF, and NI stand for excitonic insulator, antiferromagnetic excitonic insulator, and nonmagnetic insulator, respectively.

considered as the Van Vleck-type excitonic insulator induced by mixing the nonmagnetic $J = 0$ state and the magnetic $J = 1$ and $J = 2$ excited states. This is simply because $\langle \mathbf{J}^2 \rangle > 2$ is possible only when the $J = 2$ state is involved. Indeed, we can readily show that the finite order parameter $\Delta^{3/2,\pm 1/2}_{1/2,\pm 1/2}$ generates the mixing between the $J = 0$ singlet and the $J = 2$ quintets in addition to the $J = 1$ triplets. Therefore, this magnetic excitonic insulator is similar to the one proposed by Khaliullin [35] except that here the $J = 2$ quintets is also involved.

The difference between the two excitonic insulators arises from the viewpoint of multipole. The multipole momentum is described by the total angular momentum J_α $(\alpha = x, y, z)$ defined in Eq. (10), where the site index i is omitted. In the DMFT calculations, we consider eight types of multipoles, which are classified into three categories according to the irreducible representations in the cubic symmetry [47]. The first category is lowest-order three Γ_{4u} dipoles

$$J_x, \quad J_y, \quad J_z. \tag{11}$$

The second category is two Γ_{3g} quadrupoles

$$O_u = \frac{1}{2}\left(2J_z^2 - J_x^2 - J_y^2\right), \quad O_v = \frac{\sqrt{3}}{2}\left(J_x^2 - J_y^2\right). \tag{12}$$

The third category is three Γ_{5g} quadrupoles

$$O_{xy} = \frac{\sqrt{3}}{2}(J_x J_y + J_y J_x), \quad O_{yz} = \frac{\sqrt{3}}{2}(J_y J_z + J_z J_y),$$
$$O_{zx} = \frac{\sqrt{3}}{2}(J_z J_x + J_x J_z). \tag{13}$$

As shown in Fig. 4(a), for the magnetic excitonic insulator with large U, J_z is finite, which signals the dipole ordering. On the other hand, it is noticed in Fig. 4(b) that for the nonmagnetic excitonic insulator with moderate U, all the dipole orderings disappear but the O_u component of the Γ_{3g} quadrupole moments becomes clearly dominant, revealing the quadrupole order in the nonmagnetic excitonic insulator. We should note that the same component of the Γ_{3g} quadrupole moments is finite even in the magnetic excitonic insulator with large U. This is understood simply because the lower-order dipole moment is finite. As shown in Fig. 4(a), in this magnetic excitonic insulator, J_z is finite but $J_x = J_y = 0$ in Γ_{4u} dipoles, and thus we can easily show that the O_u component of the two-dimensional Γ_{3g} quadrupoles is also finite among $\Gamma_{4u} \times \Gamma_{4u} = \Gamma_{1g} + \Gamma_{3g} + \Gamma_{4g} + \Gamma_{5g}$ (except for Γ_{1g}), as we have indeed found in our calculations.

V. SINGLE-PARTICLE SPECTRA

Finally, we calculate the momentum-resolved single-particle spectral function

$$A(k, \omega) = -\frac{1}{\pi} \sum_{j,m} \mathrm{Im}\mathcal{G}^{j,m}_{j,m}(k, \omega + i0^+) \tag{14}$$

and examine the characteristic features in the single-particle excitations for the different insulating states found here. In our calculations, the single-particle Green's function $\mathcal{G}^{j,m}_{j,m}(k, \omega)$ is introduced within the cluster perturbation theory [48]. Since the DMFT can include the momentum k dependence only through the noninteracting energy dispersion $\epsilon(k)$, we introduce k to parametrize $\epsilon(k)$ as $\epsilon(k) = -2\cos k$ [49].

The typical results of $A(k, \omega)$ are summarized in Fig. 5 for the four different insulators. As shown in Fig. 5(a), $A(k, \omega)$ for the relativistic band insulator in the moderate correlation regime is very similar to the noninteracting band structure for large λ and exhibits an indirect gap between the $j = 1/2$ and $3/2$ based bands. With slightly decreasing the SOC, the ground state becomes the nonmagnetic excitonic insulator with the quadrupole order and the typical result of $A(k, \omega)$ is shown in Fig. 5(b). This result clearly demonstrates the strong hybridization between the bottom of the $j = 1/2$ based conduction band and the top of the $j = 3/2$ based valence bands to induce a finite excitation gap at the Fermi energy, and this is a strong evidence for the excitonic insulator [see also Fig. 3(b)]. It is also noticed in Fig. 5(b) that the spectrum is rather broad, as compared with the one for the relativistic band insulator shown in Fig. 5(a), despite that U is the same for both cases.

Figure 5(c) represents the result for the Van Vleck-type insulator that appears in the strong correlation regime. The apparent difference from the moderate correlation regime is that the single-particle excitation gap is determined by U and the spectrum is rather featureless with a much broader structure specially in the occupied states below the Fermi energy. The typical result for the magnetic excitonic insulator is shown in Fig. 5(d). Similar to the Van Vleck-type insulator, $A(k, \omega)$ exhibits a broad structure. In addition, there exists a characteristic peak structure near $\omega = 0$ below the Fermi energy. The dispersion of this excitation is strongly renormalized to become almost flat, implying the strong correlation effects. As shown in Fig. 2(b), this excitation originates mainly from the one with the $m = \pm 1/2$ character of $j = 3/2$, the four-fold degeneracy of $j = 3/2$ being lifted due to the magnetic excitonic order.

VI. SUMMARY

In summary, we have studied the three-orbital Hubbard model with the SOC at four electrons per site by using the

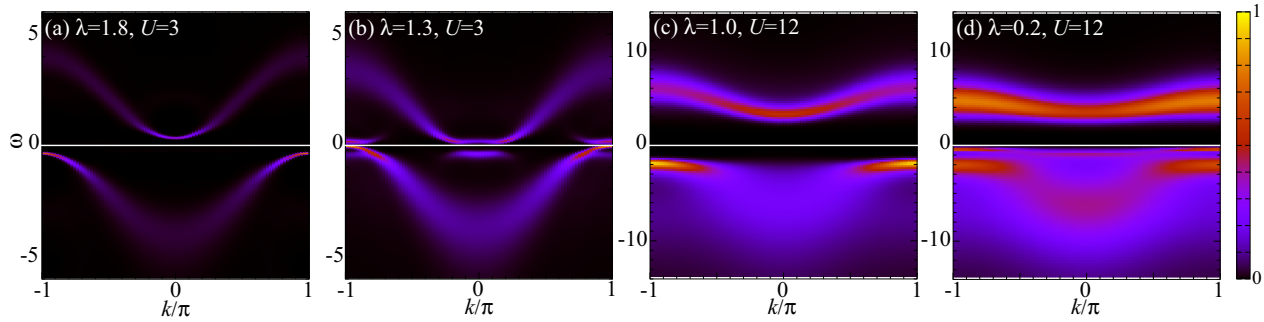

FIG. 5. k-resolved single-particle spectral function $A(k,\omega)$ for (a) relativistic band insulator, (b) nonmagnetic excitonic insulator with the quadrupole order, (c) Van Vleck-type nonmagnetic insulator, and (d) magnetic excitonic insulator. The parameters are indicated in the figures. (a) and (c) are in the "NI" phase, (b) is in the "EXI" phase, and (d) is in the "EXI+AF" phase of the phase diagram shown in Fig. 1. Note that the maximum value of each spectral function is normalized to be one. The Fermi energy is denoted by white horizontal lines at $\omega = 0$.

multiorbital DMFT and the CTQMC method. For large U, we have demonstrated that the moderate SOC induces the Van Vleck-type nonmagnetic insulator, which is smoothly connected to the relativistic band insulator for larger λ. We have also found in the strong electron correlation regime that the magnetic excitonic insulator is induced for small λ by hybridizing the nonmagnetic $J = 0$ singlet of the local $(t_{2g})^4$ manifold and the excited multiplets with $J = 1$ triplets and $J = 2$ quintets. More interestingly, we have found that the excitonic insulator for moderate U emerges without any magnetic order. This excitonic insulator is due to the condensation of an electron-hole pair in the $j = 1/2$ and $3/2$ based bands, and is characterized by the high-order Γ_{3g} quadrupole order. Although our results for moderate U are most appropriate for $5d$ transition-metal oxides, the results for large U should also be relevant to $3d$ and $4d$ transition-metal oxides with the low spin configuration in the cubic O_h symmetry. The different insulators found here are manifested most clearly in the momentum-resolved single-particle excitations, and thus can be observed in angle-resolved photoemission spectroscopy experiments.

ACKNOWLEDGMENTS

The authors are grateful to K. Seki and B. H. Kim for valuable discussion. Most of the numerical computations have been performed with facilities at Supercomputer Center in ISSP, Information Technology Center, University of Tokyo, and with the RIKEN supercomputer system (HOKUSAI GreatWave). The calculations have also been performed in part with K computer at RIKEN Center for Computational Science (R-CCS) through the HPCI System Research project (project ID.: hp150140). This work has been supported by Grant-in-Aid for Scientific Research from MEXT Japan under the Grant No. 25287096. T. Sato acknowledges the Deutsche Forschungsgemeinschaft for financial support (Grant No. AS120/14-1). T. Shirakawa acknowledges Simons Foundation for financial support (Award No. 534160).

[1] G. Cao and P. Schlottmann, Rep. Prog. Phys. **81**, 042502 (2018).
[2] J. J. Randall, L. Katz, and R. Ward, J. Am. Chem. Soc. **79**, 266 (1957).
[3] R. J. Cava, B. Batlogg, K. Kiyono, H. Takagi, J. J. Krajewski, W. F. Peck, Jr., L. W. Rupp, Jr., and C. H. Chen, Phys. Rev. B **49**, 11890 (1994).
[4] T. Shimura, Y. Inaguma, T. Nakamura, M. Itoh, and Y. Morii, Phys. Rev. B **52**, 9143 (1995).
[5] G. Cao, J. Bolivar, S. McCall, J. E. Crow, and R. P. Guertin, Phys. Rev. B **57**, 11039(R) (1998).
[6] B. J. Kim, H. Jin, S. J. Moon, J.-Y. Kim, B.-G. Park, C. S. Leem, J. Yu, T. W. Noh, C. Kim, S.-J. Oh, J.-H. Park, V. Durairaj, G. Cao, and E. Rotenberg, Phys. Rev. Lett. **101**, 076402 (2008).
[7] B. J. Kim, H. Ohsumi, T. Komesu, S. Sakai, T. Morita, H. Takagi, and T. Arima, Science **323**, 1329 (2009).
[8] K. Ishii, I. Jarrige, M. Yoshida, K. Ikeuchi, J. Mizuki, K. Ohashi, T. Takayama, J. Matsuno, and H. Takagi, Phys. Rev. B **83**, 115121 (2011).
[9] H. Okabe, M. Isobe, E. Takayama-Muromachi, A. Koda, S. Takeshita, M. Hiraishi, M. Miyazaki, R. Kadono, Y. Miyake, and J. Akimitsu, Phys. Rev. B **83**, 155118 (2011).
[10] J. Kim, D. Casa, M. H. Upton, T. Gog, Y.-J. Kim, J. F. Mitchell, M. van Veenendaal, M. Daghofer, J. van den Brink, G. Khaliullin, and B. J. Kim, Phys. Rev. Lett. **108**, 177003 (2012).
[11] S. Fujiyama, H. Ohsumi, T. Komesu, J. Matsuno, B. J. Kim, M. Takata, T. Arima, and H. Takagi, Phys. Rev. Lett. **108**, 247212 (2012).
[12] Y. Liu, L. Yu, X. Jia, J. Zhao, H. Weng, Y. Peng, C. Chen, Z. Xie, D. Mou, J. He, X. Liu, Y. Feng, H. Yi, L. Zhao, G. Liu, S. He, X. Dong, J. Zhang, Z. Xu, C. Chen, G. Cao, X. Dai, Z. Fang, and X. J. Zhou, Sci. Rep. **5**, 13036 (2015).
[13] G. Jackeli and G. Khaliullin, Phys. Rev. Lett. **102**, 017205 (2009).
[14] H. Jin, H. Jeong, T. Ozaki, and J. Yu, Phys. Rev. B **80**, 075112 (2009).
[15] H. Watanabe, T. Shirakawa, and S. Yunoki, Phys. Rev. Lett. **105**, 216410 (2010).

[16] F. Wang and T. Senthil, Phys. Rev. Lett. **106**, 136402 (2011).
[17] C. Martins, M. Aichhorn, L. Vaugier, and S. Biermann, Phys. Rev. Lett. **107**, 266404 (2011).
[18] T. Shirakawa, H. Watanabe, and S. Yunoki, J. Phys.: Conf. Ser. **273**, 012148 (2011).
[19] R. Arita, J. Kuneš, A. V. Kozhevnikov, A. G. Eguiluz, and M. Imada, Phys. Rev. Lett. **108**, 086403 (2012).
[20] H. Onishi, J. Phys.: Conf. Ser. **391**, 012102 (2012).
[21] H. Watanabe, T. Shirakawa, and S. Yunoki, Phys. Rev. Lett. **110**, 027002 (2013).
[22] Z. Y. Meng, Y. B. Kim, and H.-Y. Kee, Phys. Rev. Lett. **113**, 177003 (2014).
[23] Y. Yang, W.-S. Wang, J.-G. Liu, H. Chen, J.-H. Dai, and Q.-H. Wang, Phys. Rev. B **89**, 094518 (2014).
[24] H. Watanabe, T. Shirakawa, and S. Yunoki, Phys. Rev. B **89**, 165115 (2014).
[25] T. Sato, T. Shirakawa, and S. Yunoki, Phys. Rev. B **91**, 125122 (2015).
[26] S. Zhou, K. Jiang, H. Chen, and Z. Wang, Phys. Rev. X **7**, 041018 (2017).
[27] Y. Shi, Y. Guo, Y. Shirako, W. Yi, X. Wang, A. A. Belik, Y. Matsushita, H. L. Feng, Y. Tsujimoto, M. Arai, N. Wang, M. Akaogi, and K. Yamaura, J. Am. Chem. Soc. **135**, 16507 (2013).
[28] P. Zheng, Y. G. Shi, A. F. Fang, T. Dong, K. Yamaura, and N. L. Wang, J. Phys.: Condens. Matter **26**, 435601 (2014).
[29] M. Bremholm, S. E. Dutton, P. W. Stephens, and R. J. Cava, J. Solid State Chem. **184**, 601 (2011).
[30] L. Du, X. Sheng, H. Weng, and X. Dai, Europhys. Lett. **101**, 27003 (2013).
[31] L. Du, L. Huang, and X. Dai, Eur. Phys. J. B **86**, 94 (2013).
[32] M.-C. Jung and K.-W. Lee, Phys. Rev. B **90**, 045120 (2014).
[33] T. Dey, A. Maljuk, D. V. Efremov, O. Kataeva, S. Gass, C. G. F. Blum, F. Steckel, D. Gruner, T. Ritschel, A. U. B. Wolter, J. Geck, C. Hess, K. Koepernik, J. van den Brink, S. Wurmehl, and B. Büchner, Phys. Rev. B **93**, 014434 (2016).
[34] S. Fuchs, T. Dey, G. Aslan-Cansever, A. Maljuk, S. Wurmehl, B. Büchner, and V. Kataev, Phys. Rev. Lett. **120**, 237204 (2018).
[35] G. Khaliullin, Phys. Rev. Lett. **111**, 197201 (2013).
[36] G. Kotliar, S. Y. Savrasov, G. Pálsson, and G. Biroli, Phys. Rev. Lett. **87**, 186401 (2001).
[37] J. Kanamori, Prog. Theor. Phys. **30**, 275 (1963).
[38] See also E. Dagotto, T. Hotta, and A. Moreo, Phys. Rep. **344**, 1 (2001).
[39] D. van der Marel and G. A. Sawatzky, Phys. Rev. B **37**, 10674 (1988).
[40] A. Georges, L. de'Medici, and J. Mravlje, Annu. Rev. Condens. Matter Phys. **4**, 137 (2013).
[41] W. Metzner and D. Vollhardt, Phys. Rev. Lett. **62**, 324 (1989).
[42] M. Eckstein, M. Kollar, K. Byczuk, and D. Vollhardt, Phys. Rev. B. **71**, 235119 (2005).
[43] P. Werner, A. Comanac, L. de Medici, M. Troyer, and A. J. Millis, Phys. Rev. Lett. **97**, 076405 (2006).
[44] This is also the case for another excitonic insulating phase indicated as "EXI" in the phase diagram shown in Fig 1.
[45] M. Jarrell and J. E. Gubernatis, Phys. Rep. **269**, 133 (1996).
[46] C. Svoboda, M. Randeria, and N. Trivedi, Phys. Rev. B **95**, 014409 (2017).
[47] H. Onishi, J. Phys. Soc. Jpn. **80**, SA141 (2011).
[48] D. Sénéchal, D. Perez, and M. Pioro-Ladriére, Phys. Rev. Lett. **84**, 522 (2000).
[49] S. Hoshino, J. Otsuki, and Y. Kuramoto, J. Phys. Soc. Jpn. **82**, 044707 (2013).